ACS Medicinal Chemistry Letters

Letter

pubs.acs.org/acsmedchemlett

Discovery of the Highly Potent PI3K/mTOR Dual Inhibitor PF-04979064 through Structure-Based Drug Design

Hengmiao Cheng,*[,†] Chunze Li,[‡] Simon Bailey,[†] Sangita M. Baxi,[§] Lance Goulet,[‡] Lisa Guo,[†] Jacqui Hoffman,[†] Ying Jiang,[‡] Theodore Otto Johnson,[†] Ted W. Johnson,[†] Daniel R. Knighton,[†] John Li,[§] Kevin K.-C. Liu,[†] Zhengyu Liu,[†] Matthew A. Marx,[†] Marlena Walls,[§] Peter A. Wells,[§] Min-Jean Yin,[§] Jinjiang Zhu,[†] and Michael Zientek[‡]

[†]Cancer Chemistry, [‡]PDM, and [§]Oncology Research Unit, Pfizer Worldwide Research and Development, La Jolla Laboratories, 10770 Science Center Drive, San Diego, California 92121, United States

Supporting Information

ABSTRACT: PI3K, AKT, and mTOR are key kinases from PI3K signaling pathway being extensively pursued to treat a variety of cancers in oncology. To search for a structurally differentiated back-up candidate to PF-04691502, which is currently in phase I/II clinical trials for treating solid tumors, a lead optimization effort was carried out with a tricyclic imidazo[1,5]naphthyridine series. Integration of structure-based drug design and physical properties-based optimization yielded a potent and selective PI3K/mTOR dual kinase inhibitor PF-04979064. This manuscript discusses the lead optimization for the tricyclic series, which both improved the in vitro potency and addressed a number of ADMET issues including high metabolic clearance mediated by both P450 and aldehyde oxidase (AO), poor permeability, and poor solubility. An empirical scaling tool was developed to predict human clearance from in vitro human liver S9 assay data for tricyclic derivatives that were AO substrates.

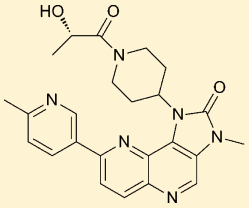

KEYWORDS: *PF-04979064, kinase inhibitor, PI3K/mTOR dual inhibitor, aldehyde oxidase metabolism, cancer, antitumor*

The phosphatidylinositol 3-kinase (PI3K) signaling pathway plays crucial roles in cell growth, proliferation, and survival and is a frequently dysregulated pathway in human cancers.[1,2] Inhibitors of key kinases in the pathway, including PI3K, AKT, and mTOR, have been extensively pursued in oncology in recent years.[3] Because PI3K/mTOR dual inhibitors may most effectively block the PI3K pathway, overcome feedback loops,[4] and block PI3K-independent mTOR activation, our strategy to target PI3K signaling pathway was focused on PI3K/mTOR dual inhibitors. Two highly potent and selective ATP competitive kinase inhibitors of class 1 PI3Ks and mTOR from Pfizer, an oral agent PF-04691502[5,6] and an iv-administered agent PF-05212384 (PKI-587),[7] are currently in phase I/II clinical trials for the treatment of solid tumors (Figure 1).

PF-04691502 is derived from the 4-methylpyridopyrimidinone series. In our search for a structurally differentiated back-up candidate to PF-04691502, compound **1**, from a tricyclic imidazo[1,5]naphthyridine series[8,9] that was designed through a fast follower approach to BEZ235,[10] was identified as an interesting lead. It exhibited potent in vitro activity against mouse PI3Kα,[5] which was used as a surrogate of human PI3Kα in the primary screening, with a K_i of 1.41 nM, which translates to a ligand efficiency (LE) of 0.354. When tested in an mTOR kinase domain in vitro biochemical assay, **1** also exhibited good activity with a K_i of 4.51 nM. In a BT20 cell assay, measuring inhibition of AKT phosphorylation at S473, **1** exhibited moderate cellular potency with an IC_{50} of 144 nM.

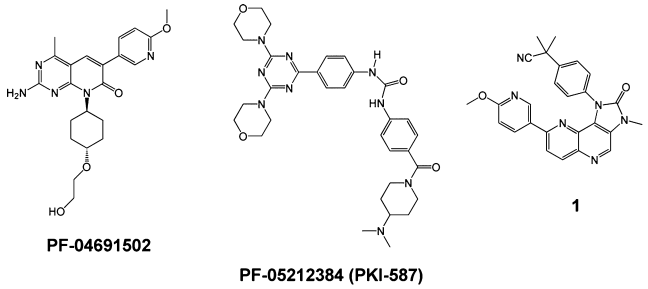

Figure 1. Chemical structures of PF-04691502, PF-05212384, and the new lead **1**.

Shown in Scheme 1 is the general synthetic route for preparing the tricyclic derivatives discussed in this paper.[11] Readily available starting material **2** is reacted with 2-(ethoxymethylene)-malonate at elevated temperature to afford compound **3**, which is heated in phenyl ether (Ph_2O) to afford the cyclized compound **4**. Treatment of **4** with $POCl_3$ yields 4,6-dichloro-(1,5)-naphthyridine-3-carboxylic acid ethyl ester **5**, which is subjected to Suzuki coupling conditions with a boronic acid or boronic ester derivative to give compound **6**. Compound **7** is prepared by treatment of **6** with an amine, and subsequent hydrolysis of the ester in **7** gives the free acid **8**.

Received: October 2, 2012
Accepted: November 7, 2012
Published: November 7, 2012

Scheme 1. General Synthetic Route for the Tricyclic Derivatives[a]

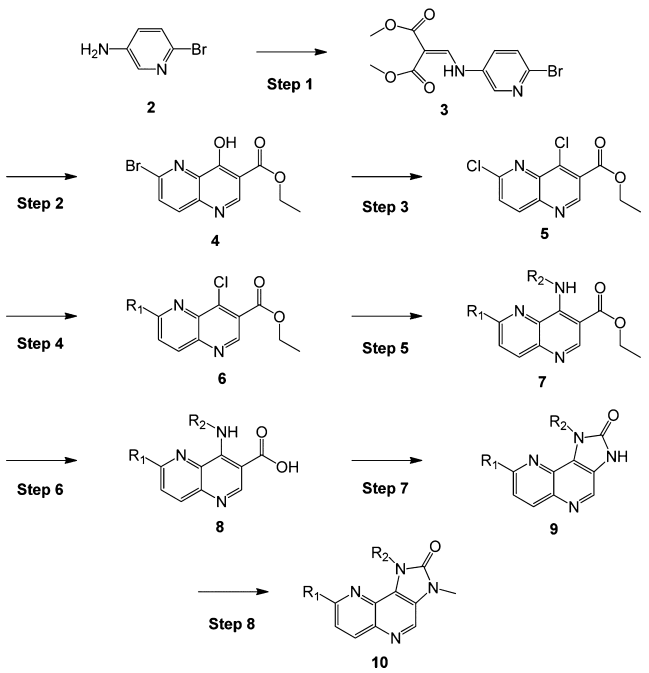

[a]Reagents: Step 1: 2-(ethoxymethylene)-malonate, ethanol, reflux. Step 2: phenyl ether, reflux. Step 3: $POCl_3$, reflux. Step 4: boronic acid/boronic ester, K_2CO_3, $Pd(PPh_3)_4$, toluene. Step 5: R_1NH_2, AcOH. Step 6: LiOH, EtOH–water. Step 7: DPPA, Et3N, DMF. Step 8: MeI, NaOH, CH_2Cl_2.

When **8** is treated with diphenylphosphoryl azide (DPPA) and Et_3N, the initially formed nitrene intermediate from Curtius rearrangement reacts with the amine at 4-naphthyridine to undergo intramolecular cyclization to produce compound **9**, which is methylated to give compound **10**. The tricyclic derivatives with acylated piperidine moieties can be prepared from **10** by first removing the protecting groups on the piperidine, followed by amide formation.

Docking studies of the tricyclic analogues with PI3Kα were carried out,[10] and the proposed binding mode for **1** is illustrated in Figure 2. The naphthyridine ring nitrogen formed a key hydrogen bond with the hinge residue Val 882. The ring nitrogen on the methoxypyridine formed a hydrogen bond with the conserved water molecule in the selectivity pocket. The phenyl group from the benzyl nitrile moiety bound in a hydrophobic pocket, and the nitrile formed a H bond with Lys 833 in the phosphate binding pocket.

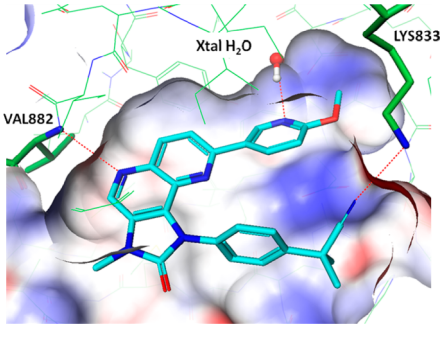

Figure 2. Modeled structure of compound **1** with PI3Kγ.

Physical properties-based optimization (PPBO) of multiple druglike attributes,[12] guided by structure-based drug design (SBDD), commenced. Compound **1** was highly lipophilic, with a clogP of 4.69, exhibiting high metabolic clearance in both HLM and RLM in vitro assays, with extraction ratios (ERs) of 0.652 and 0.724, respectively. Compound **1** demonstrated poor solubility and poor permeability, with measured kinetic solubility of 2.00 μM[5] and measured RRCK permeability of 0.305 $\times$ 10^{-6} cm/s, respectively. Even though **1** exhibited potent biochemical enzyme K_i against both mPI3Kα and mTOR, it only showed moderate cell potency; poor solubility and permeability of **1** may account for the high ratio between cell IC_{50} and mPI3Kα K_i values.

The medicinal chemistry goals for the lead optimization from **1** were to increase cell potency, metabolic stability, permeability, and solubility. Because compounds with lower clogP usually exhibit lower metabolic clearance and greater solubility,[5] the strategy to increase metabolic stability and solubility was to reduce clogP for the new designs. In addition, **1** had multiple aromatic rings, and π–π stacking of the aromatic rings could also contribute to its poor solubility. Consequently, a second strategy to increase solubility was to increase the 3D structure to minimize π–π stacking. It was reasoned that increased solubility could also lead to improved permeability, which could help reduce the ratio between cell IC_{50} and enzymatic K_i. On the basis of the docking studies, because the phenyl group off the tricyclic core in **1** bound in a hydrophobic pocket, replacing the phenyl ring with a piperidine or a cyclohexane group would both maintain the hydrophobic interactions between the methylene groups of the piperidine or cyclohaxane ring with the enzyme and increase the 3D structure. In addition, polar groups such as an amide or an alcohol could also be introduced to the piperidine or cyclohexane ring to reduce clogP and still maintain the binding affinity by forming H bonds with the polar residues in the phosphate binding pocket.

Following the above-discussed strategies and tactics, tricyclic derivatives **11**–**14** in Table 1 were designed by replacing the benzyl nitrile moiety with substituted cyclohexane and piperidine derivatives. The clogP for these compounds ranged from 1.07 to 2.37. Data for **1** are shown in Table 1 for comparison. Overall, these compounds exhibited increased permeability and cellular potency. Significant increases in lipophilic efficiency (LipE = pIC_{50} – clogP)[5] were achieved because clogP was significantly reduced by replacing the benzyl nitrile moiety with cyclohexane and piperidine derivatives. Metabolic clearance for compounds **12**–**14** was also reduced; however, solubility for **12** and **14** needed further improvement.

Compound **13** also exhibited relatively low intrinsic clearance in rat liver microsome assay (19.9 μL/min/mg). To determine the in vivo PK profile for a representative compound from the series, **13** was progressed to rat PK studies and exhibited favorable rat PK profile: Vdss = 4.46 L/kg, Cl = 24.2 mL/min/kg, $T_{1/2}$ = 2.43 h, and F % = 76%.

Because **13** demonstrated favorable in vitro and in vivo ADMET properties, in vitro biotransformation of **13** was conducted in human liver S9. LC-MS/MS analysis showed that **13** was predominantly metabolized to **15** (Scheme 2). In addition, it was determined that oxidation of **13** to **15** did not require NADPH, a cofactor essential for P450-mediated oxidation, and the oxidation was readily inhibited by raloxifene, an aldehyde oxidase (AO) inhibitor.[13] Together, these results indicated that AO was responsible for the oxidation of **13** to **15**. After **15** was isolated form a large scale incubation of **13** with

dx.doi.org/10.1021/ml300309h | ACS Med. Chem. Lett. 2013, 4, 91–97

Table 1. Tricyclic Derivatives

Compound ID	Structure	mTOR Ki[a] (nM)	mPI3Kα Ki[a] (nM)	pAKT IC_{50}[a] (nM)	HLM Clint (ml/min/kg)	RRCK (10^{-6} cm/sec)	Sol (μM)	clogP	LipE (Cell1IC_{50})[c]
1	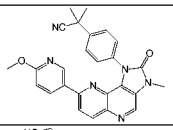	4.51	1.41	144	31.8	0.305	2.00	4.69	2.15
11	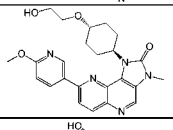	4.71	< 0.500	15.4	27.6	14.3	117	2.37	5.4
12	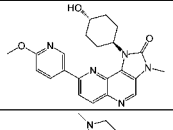	2.00	< 0.500	9.52	23.0	14.3	22.2	2.35	5.7
13	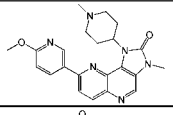	47.4	5.69	57.9	22.5	6.49	ND[b]	2.30	4.9
14	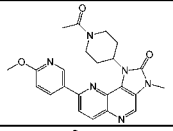	2.20	0.542	16.8	< 9.70	16.3	22.0	1.07	6.7
16	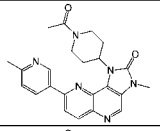	2.33	1.97	31.6	< 9.76	19.5	455	0.748	6.8
17	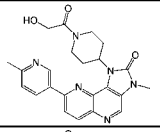	0.842	0.532	17.3	< 8.81	18.2	ND[b]	0.962	6.8
18	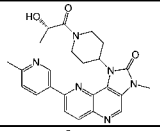	1.42	0.299	9.10	< 10.3	17.2	539	1.27	6.8
19	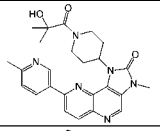	18.5	3.89	22.5	10.7	21.9	ND[b]	1.58	6.1
20	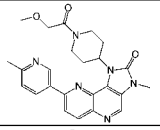	0.377	0.922	11.1	17.9	20.2	ND[b]	1.21	6.7
21	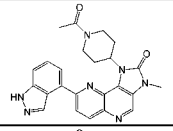	1.55	0.584	31.5	< 10.4	8.56	55.5	1.16	6.3
22	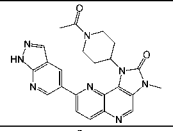	0.243	0.191	11.6	22.6	3.97	ND[b]	0.428	7.5
23	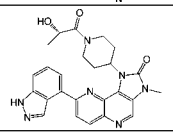	2.64	0.395	28.3	< 9.73	4.60	444	1.68	5.9

[a]Inhibition constants (K_i) and cell IC_{50} values were determined as described in refs 5 and 6. The coefficients of variance were typically less than 20% (n = 2). [b]Data not determined. [c]LipE (IC_{50}) = pIC_{50} − clogP.

dx.doi.org/10.1021/ml300309h | ACS Med. Chem. Lett. 2013, 4, 91−97

Scheme 2. AO Oxidation of 13

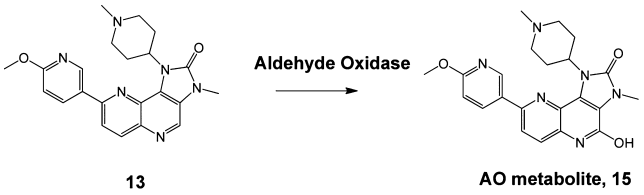

human S9, its structure was determined by ^{1}H NMR analysis, confirming that the tricyclic core was the site of oxidation, consistent with the oxidative characteristics for AO.[14] Because AO is a cytosolic enzyme, the stability of **13** was evaluated in a human liver S9 assay.[15] Indeed, **13** was rapidly cleared in vitro in human liver S9 with a half-life of 6.5 min.

Human PK prediction for P450-metabolized compounds has become a well-established and integrated process in lead optimization. However, for AO-metabolized compounds, human PK prediction remains a challenge because there is marked species differences in AO expression and there is no established in vitro and in vivo scaling method to calculate human clearance.[15] Even though compound **13** exhibited a robust PK profile in rat, with its short half-life in human liver S9 assay, confidence for a robust human PK for **13** was low.

To select a compound with robust predicted human PK as a back-up to PF-04691502, a strategy to reduce the rate of AO oxidation to improve human PK was pursued. One way to reduce the AO oxidation rate is to disrupt the binding by increasing the bulkiness of the molecule.[16] Compound **14** in Table 1 demonstrated the highest LipE and promising overall profile; hence, it was selected as the basis for the next round of designs.

Guided by SBDD, the methoxypyridine in **14** was replaced both by methylpyridine and by bicyclic heterocycles, and the acetyl group was substituted with an alcohol or an ether. These modifications would both increase bulkiness to reduce AO clearance and be tolerated with regard to in vitro potency because additional H bonds could be formed with the protein polar residues. Data for these designs, that is, compounds **16**–**23**, are summarized in Table 1. These compounds exhibited good in vitro potency and good permeability. Low HLM clearance mediated by P450 was also observed for all of the compounds except compounds **20** and **22**, which exhibited moderate clearance. As compared with **14**, the follow-on designs also exhibited significantly increased solubility. The primary alcohol **17**, the secondary alcohol **18**, and the methylether **20** demonstrated increased potency against both mPI3Kα and mTOR. The tertiary alcohol **19** exhibited reduced binding affinity in the enzyme assays, probably due to unfavorable steric interactions between the bulky tertiary alcohol moiety and the proteins. Of the compounds containing bicyclic heterocycle side chains, **22** with the pyrazolopyridine side chain exhibited highly potent K_i against both mPI3Kα and mTOR. However, **22** showed low permeability and, consequently, a high ratio between cell IC_{50} and K_i.

Compound **18** demonstrated the best overall properties including the most potent cell IC_{50}, low HLM clearance, high permeability, and very good solubility. A crystal structure of **18** bound with PI3Kγ was subsequently determined (Figure 3). The naphthyridine ring nitrogen of **18** bound in the hinge region, the methylpyridine nitrogen formed H bond with the conserved water molecule, and two additional H bonds were also formed between the amide carbonyl from **18** and Lys 833

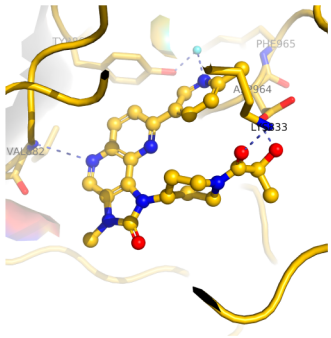

Figure 3. Cocrystal structure of **18** with PI3Kγ.

side chain and between the alcohol from **18** and the Asp 964 side chain. The binding mode of **18** in PI3Kγ, determined by crystal structure, is consistent with the modeled binding mode of compound **1** in PI3Kγ.

Six compounds from Table 1 were selected and tested in human liver S9 assay to determine their AO oxidation rate, and the half-lives are summarized in Table 2. For example, $T_{1/2}$ for

Table 2. AO Half Lives from in Vitro Human Liver S9 Assay

compd ID	human S9 $T_{1/2}$ (min)	compd ID	human S9 $T_{1/2}$ (min)
16	8.60	**19**	12.2
17	21.9	**21**	158
18	38.7	**23**	156

18 is 38.7 min, which is significantly longer than that of **13**. Furthermore, the indazole derivatives **21** and **23** are found to exhibit longer than 150 min half-lives. The data suggest that it is a validated strategy to reduce AO metabolism rate by increasing the size of the compounds to decrease their binding affinity with AO.

With several tricyclic compounds that exhibited reduced AO clearance and met other project progression criteria, to prioritize them for in vivo studies, a strategy to predict their human clearance was developed. The conventional methods, including in vitro metabolic scaling and allometric scaling from preclinical species, have not successfully predicted human clearance for AO substrates. It was reported by Zientek[15] that when in vitro S9 and cytosol stability data were used for metabolic scaling, the rank order of scaled intrinsic clearance was generally aligned between in vitro and in vivo data; however, the in vivo clearance for almost every compound evaluated was underestimated, with an average of 11-fold for the under estimation. Recently, Hutzler[17] and Akabane[18] reported a similar trend for metabolic scaling of AO substrates from stability data in cryopreserved human hepatocytes and custom pooled hepatocytes, respectively. An underestimation of 7.9–14.9-fold was reported by Akabane for the AO substrates.[18] With AO clearance half-life determined for the tricyclic compounds from human liver S9 assay, we decided to build an empirical calibration curve for human clearance for AO substrates to describe the relationship between observed human clearance and clearance predicted by metabolic scaling method.[8,9] Four known AO substrates with reported human pharmacokinetic data, namely, carbazeran,[19] zoniporide,[20] zaleplon,[21] and PF-04217903,[22] were selected to build an empirical calibration curve for human clearance for AO substrates to describe the relationship between observed human clearance and clearance predicted by metabolic scaling

dx.doi.org/10.1021/ml300309h | ACS Med. Chem. Lett. 2013, 4, 91–97

method.[8,9] As shown in Table 3, these four compounds covered a broad range of stability (1−162 min) in human liver S9 in the presence of NADPH, which was included to capture both AO- and P450-mediated clearance in the incubations.

Table 3. Summary of Calculated Hepatic Plasma Clearance of AO Substrates in Human S9 as Compared with Reported Human Clearances

					mL/min/kg	
compd	$T_{1/2}$ in S9 (NADPH) (min)	fu,p	blood/ plasma ratio	fu,HS9 in silico	calcd $CL_{H,P}$[a]	obsd total CL_p[b]
carbazeran	1.01	0.08	0.70	0.735	10.6	38
zoniporide	20.8	0.34	0.75	0.753	5.1	21
zaleplon	64.3	0.49	0.74	0.548	3.7	16
PF-04217903	162	0.16	0.90	0.912	0.40	6

[a]Calculated $CL_{H,P}$ was calculated using the three equations described in the manuscript. [b]Observed intravenous plasma clearance except PF-04217903. The intravenous clearance of PF-04217903 was estimated based on observed oral clearance and physiological-based pharmacokinetic modeling.

To estimate the hepatic plasma clearance ($CL_{H,P}$), the in vitro unbound intrinsic clearance ($CL_{int,u}$) was first estimated from the in vitro human S9 stability data using eq 1, where $t_{1/2}$ is the observed in vitro substrate depletion half-life (in min). As AO substrates were not stable in human S9, protein binding in human S9 could not be measured experimentally. Hence, protein binding of AO substrates was estimated by Pfizer in-house in silico models.

$$CL_{int,u} = 0.693 \times \frac{1}{t_{1/2}} \times \frac{\text{mL incubation}}{\text{5 mg of S9}} \times \frac{1}{f_{u,HS9}} \times \frac{\text{120 mg of S9}}{\text{g of liver}} \times \frac{\text{21 g of liver}}{\text{kg of BW}} \quad (1)$$

Human hepatic blood clearance ($CL_{H,B}$) was calculated using $CL_{int,u}$ values and well-stirred model according to eq 2, where Q_H is human hepatic blood flow (21 mL/min/kg) and $f_{u,B}$ is fraction unbound in human blood. Hepatic plasma clearance ($CL_{H,P}$) was calculated following eq 3.

$$CL_{H,B} = \frac{Q_H \times f_{u,B} \times CL_{int,u}}{Q_H + (f_{u,B} \times CL_{int,u})} \quad (2)$$

$$CL_{H,P} = CL_{H,B} \times \text{blood to plasma ratio} \quad (3)$$

Consistent with Zientek's finding, $CL_{H,P}$ calculated by metabolic scaling from in vitro data underestimated the observed human clearance for the four AO substrates tested (Table 3). Additional analysis was conducted to explore the relationship between the calculated and the observed clearances. As shown in Figure 4, a linear relationship was observed between calculated and observed plasma clearances for the four known AO substrates, which provided us an empirical scaling tool to predict human clearance for tricyclic compounds using in vitro human S9 stability data.

Human clearance was then predicted for the tricyclic derivatives by using the above-discussed linear calibration curve, and compounds **18** and **23** emerged as two leads with acceptable predicted human clearance, which is summarized in Table 4. These compounds were progressed to mouse PK and

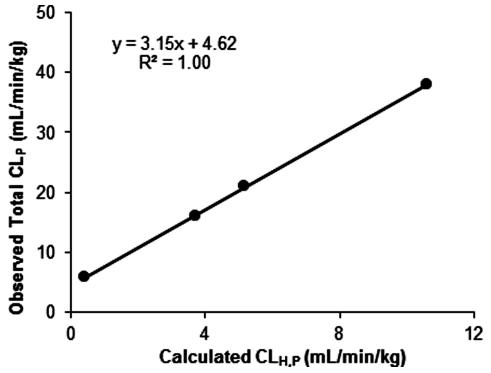

Figure 4. Calibration curve of AO substrates between observed total CL_p and calculated $CL_{H,P}$ based on in vitro stability data.

Table 4. Predicted Human Clearance for the Top Two Tricyclic Derivatives

					mL/min/kg	
compd	$T_{1/2}$ in S9 (NADPH) (min)	fu,p	blood/ plasma ratio	fu,HS9 in silico	calcd $CL_{H,P}$[a]	predicted total CL_p
18	38.7	0.0875	0.86	0.670	1.1	8.1
23	156	0.101	1.01	0.593	0.38	5.8

[a]Calculated $CL_{H,P}$ was calculated using the three equations described in the manuscript.

PK/PD studies. On the basis of the overall attributes including potency from in vitro biochemical mPI3Kα and mTOR assays and cellular assay, kinome selectivity, cerep broad ligand binding selectivity, predicted human clearance, and mouse PK/PD study results, **18** was selected to progress to mouse in vivo xenograft efficacy studies. As illustrated in Figure 5, **18**

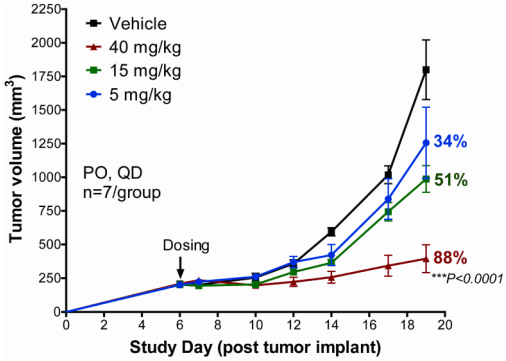

Figure 5. Tumor growth inhibition by **18** in U87MG mouse xenograft model.

exhibited dose proportional tumor growth inhibition (TGI) in a U87MG mouse xenograft model, achieving 88% TGI at the highest tolerated dose, 40 mg/kg QD.[23] Figure 6 shows that a robust in vivo PK/PD correlation for **18** was observed for samples from the high dose treatment group in the TGI studies.[24] At 1 h time point, high free drug concentration in plasma yielded maximum inhibition of AKT phosphorylation. At 24 h time point, very low free drug concentration in plasma was correlated with minimum inhibition of AKT phosphorylation.[6]

Compound **18** was tested against human class I PI3K isoforms α, γ, and δ, with PI3Kα K_i of 0.130 nM, PI3Kγ K_i of

dx.doi.org/10.1021/ml300309h | ACS Med. Chem. Lett. 2013, 4, 91−97

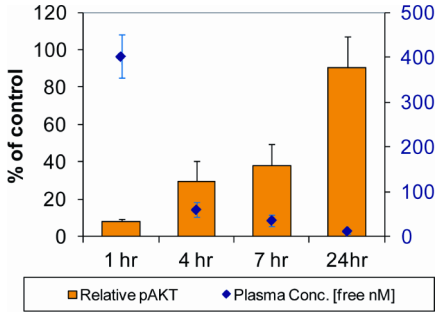

Figure 6. PK/PD correlation for **18**.

0.111 nM, and PI3Kδ K_i of 0.122 nM.[25] Compound **18** was progressed to rat in vivo PK studies and exhibited robust PK profile: Vdss = 5.23 L/kg, Cl = 19.3 mL/min/kg, $T_{1/2}$ = 1.85 h, and F % = 61%.

Shown in Figure 7 is a LipE plot to summarize the lead optimization process. In the plot, the X-axis represents clogP,

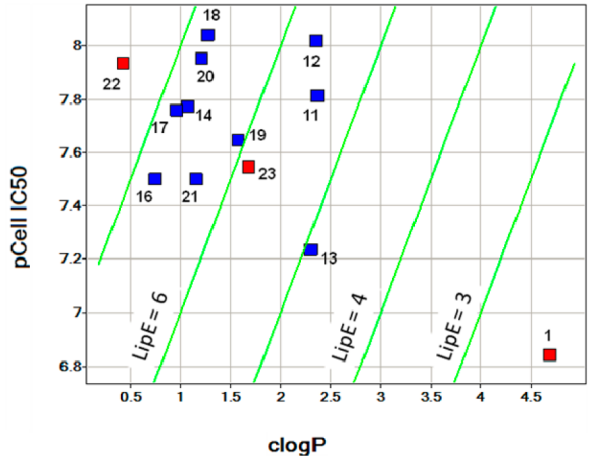

Figure 7. LipE plot to summarize the lead optimization.

the Y-axis represents p(cell IC_{50}), and the markers are colored by RRCK value, wherein a blue color indicates RRCK > 5 × 10^{-6} cm/s, and red indicates RRCK value < 5 × 10^{-6} cm/s. In general, compounds with higher LipE are desired since they usually exhibit better in vivo properties.[5] Compound **1** has high clogP, poor solubility, and high metabolic clearance. Through integration of SBDD and PPBO, **18** (PF-04979064) was discovered. As the spotfire plot illustrates, from compound **1** to PF-04979064, the LipE is increased by greater than 4 units. PF-04979064 exhibited excellent in vitro potency, very good solubility, high LipE, excellent kinome selectivity,[26] robust PK/PD correlation and TGI efficacy, and acceptable predicted human clearance after incorporating both CYP- and AO-mediated metabolism. PF-04979064 was identified as a back-up candidate to PF-04691502.

■ ASSOCIATED CONTENT

Supporting Information

Invitrogen KSS data and % inhibition at 1 μM PF-04979064 tested at ATP concentration = K_m. This material is available free of charge via the Internet at http://pubs.acs.org.

Accession Codes

The PDB accession code for the X-ray cocrystal structure of PI3Kγ + PF-04979064 is 4HVB.

■ AUTHOR INFORMATION

Corresponding Author

*Tel: 1-858-622-3208. E-mail: henry.cheng@pfizer.com.

Notes

The authors declare no competing financial interest.

■ ACKNOWLEDGMENTS

Hieu Lam and Aihua Zou are acknowledged for biochemical screenings. Xiao-hong Yu is acknowledged for cellular screenings. Ya-Li Deng and Alexei Brooun are acknowledged for preparing crystals of PF-04979064 with PI3Kγ. Ketan Gajiwala is acknowledged for preparing Figure 3 and depositing the X-ray crystal structure. Jian Lin is acknowledged for running human liver cytosol assay for the selected tricyclic derivatives.[27]

■ REFERENCES

(1) Eagleman, J. A.; Luo, J.; Cantley, L. C. The evolution of phosphatidylinositol 3-kinases as regulators of growth and metabolism. *Nat. Rev. Genet.* **2006**, *7*, 606−619.

(2) Samuels, Y.; Wang, Z.; Bardelli, A.; Silliman, N.; Ptak, J.; Szabo, S.; Yan, H.; Gazdar, A.; Powell, S. M.; Riggins, G. J.; Willson, J. K. V.; Markowitz, S.; Kinzler, K. W.; Vogelstein, B.; Velculescu, V. E. High frequency of mutations of the PIK3CA gene in human cancers. *Science* **2004**, *304*, 554.

(3) Shuttleworth, S. J.; Silva, F. A.; Cecil, A. R. L.; Tomassi, C. D.; Hill, T. J.; Raynaud, F. I.; Clarke, P. A.; Workman, P. Progress in the preclinical discovery and clinical development of class I and dual class I/IV phosphoinostide 3-kinase (PI3K) inhibitors. *Curr. Med. Chem.* **2011**, *18*, 2686−2714.

(4) Courtney, K. D.; Corcoran, R. B.; Engelman, J. A. The PI3K pathway as drug target in human cancer. *J. Clin. Oncol.* **2008**, *28*, 1075−1083.

(5) Cheng, H.; Bagrodia, S.; Bailey, S.; Edwards, M.; Hoffman, J.; Hu, Q.; Kania, R.; Knighton, D. R.; Marx, M. A.; Ninkovic, S.; Sun, S.; Zhang, E. Discovery of the Highly Potent PI3K/mTOR Dual Inhibitor PF-04691502 through Structure Based Drug Design. *MedChemCommun.* **2010**, *1*, 139−144 Experimental procedures for in vitro biochemical assays and cellular assay were reported in this reference.

(6) Yuan, J.; Mehta, P. P.; Yin, M.; Sun, S.; Zou, A.; Chen, J.; Rafidi, K.; Feng, Z.; Nickel, J.; Engebetsen, J.; Hallin, J.; Blasina, A.; Zheng, E.; Nguyen, L.; Sun, M.; Vogt, P. K.; McHarg, A.; Cheng, H.; Christensen, J. G.; Kan, J. L. C.; Bagrodia, S. PF-04691502, a potent and selective oral inhibitor of PI3K and mTOR kinases with antitumor activity. *Mol. Cancer Ther.* **2011**, *10*, 2189−2199 Experimental procedures for the TGI study were reported in this reference.

(7) Venkatesan, A. M.; Dehnhardt, C. M.; Delos Santos, E.; et al. Bis morpholino 1,3,5-triazine derivatives: potent, ATP-competitive phosphatidylinositol-3-kinase (PI3K)/Mammalian Target of Rapamycin (mTOR) inhibitors: discovery of PKI-587 a highly efficacious Dual Inhibitor. *J. Med. Chem.* **2010**, *53*, 2636−2645.

(8) Cheng, H.; Bagrodia, S.; Bailey, S. et al. Discovery of the potent PI3K/mTOR dual inhibitor PF-04979064. Oral presentation, MEDI-493, 240th ACS National Meeting, Boston, MA, United States, August 22−26, 2010.

(9) Cheng, H.; Bailey, S.; Baxi, S. M. et al. Structure-based drug design of PI3K/mTOR dual inhibitors and PI3K selective inhibitor from tricyclic imidazo[1,5]naphthyridine series. Poster presentation, 2011 AACR Special Conferences, Targeting PI3K/mTOR Signaling in Cancer, San Francisco, CA, United States, February 24−27, 2011.

(10) Maira, S. M.; Stauffer, F.; Brueggen, J.; Furet, P.; Schnell, C.; Fritsch, C.; Brachmann, S.; Chene, P.; De Pover, A.; Schoemaker, K.; Fabbro, D.; Gabriel, D.; Simonen, M.; Murphy, L.; Finan, P.; Sellers, W.; Garcia-Echeverria, C. Identification and characterization of NVP-BEZ235, a new orally available dual PI3K/mTor inhibitor with potent *in vivo* antitumour activity. *Mol. Cancer Ther.* **2008**, *7*, 1851−1863 The crystal structure of NVP-BEZ235 in PI3Kγ published in this paper was used as a reference for the initial docking studies for compound **1**,

using the Pfizer in-house 3D Molecular Visualization and Drug Design Tool.

(11) Cheng, H.; Johnson, T. W.; Hoffman, J. E.; Guo, L. C.; Liu, Z.; Johnson, T. O.; Liu, K. K. Preparation of imidazonaphthyridine derivatives for the use as PI3Kα inhibitors or PI3Kα/mTOR dual inhibitors, WO 2010038165 A1. Experimental procedures and NMR and MS data for all of the compounds discussed in this manuscript are included in the patent.

(12) Edwards, M. P. Integration of Structure-based Drug Design and Physical Properties-based Optimization to Produce Cancer Clinical Candidates, 2010, AACR invited oral presentation, Washington, DC.

(13) Obah, R. S. Potent inhibition of human liver aldehyde oxidase by raloxifen. *Drug Metab. Dispos.* **2004**, *32*, 89−97.

(14) Garattini, E.; Terao, M. Increasing recognition of importance of aldehyde oxidase in drug development and discovery. *Drug Metab. Rev.* **2011**, *43*, 374−386.

(15) Zientek, M.; Jiang, Y.; Youdim, K.; Obach, R. S. *Drug Metab. Dispos.* **2010**, *38*, 1322−1327 The experimental procedure for the human liver S9 assay was reported in this paper.

(16) Pryde, D. C.; Tran, T.; Jones, P.; Duckworth, J.; Howard, M.; Gardner, I.; Hyland, R.; Webster, R.; Wenham, T.; Bagal, S.; Omoto, K.; Schneider, R. P.; Lin, J. Medicinal chemistry approaches to avoid aldehyde oxidase metabolism. *Bioorg. Med. Chem. Lett.* **2012**, *22*, 2856−2860.

(17) Hutzler, M.; Yang, Y.; Albaugh, D.; Fullenwider, C. L.; Schmenk, J.; Fisher, M. B. Characterization of aldehyde oxidase enzyme activity in cryopreserved human hepatocyte. *Drug Metab. Dispos.* **2012**, *40*, 1322−1327.

(18) Akabane, T.; Gerst, N.; Masters, J. N.; Tamura, K. A quantitative approach to hepatic clearance prediction of metabolism by aldehyde oxidase using custome pooled hepatocytes. *Xenobiotics* **2012**, *42*, 863−871.

(19) Kaye, B.; Offerman, J. L.; Reid, J. L.; Elliott, H. L.; Hillis, W. S. A species difference in the presystemic metabolism of carbazeran in dog and man. *Xenobiotica* **1984**, *14*, 935−945.

(20) Dalvie., D.; Zhang, C.; Chen, W.; Smolarek, T.; Obach, R. S.; Loi, C. M. Cross-species comparison of the metabolism and excretion of zoniporide: Contribution of aldehyde oxidase to interspecies differences. *Drug Metab. Dispos.* **2010**, *38*, 641−654.

(21) Rosen, A. S.; Fournie, P.; Darwish, M.; Danjou, P.; Troy, S. M. Zaleplon pharmacokinetics and absolute bioavailability. *Biopharm Drug Dispos.* **1999**, *20*, 171−175.

(22) Data from Pfizer in-house file.

(23) U87MG tumor cells were subcutaneously implanted to nude mice, tumor-bearing mice were randomized and orally dosed once daily, and tumor sizes were measured and plotted. The tumor growth inhibition (TGI) was calculated as previously described[6] and indicated on the graph for each treatment group. One-way ANOVA analysis was performed to compare treated groups to vehicle group. *** represents $P < 0.0001$.

(24) U87MG tumor-bearing mice were dosed with PF-04979064 at 40 mg/kg once, and tumors were harvested at various time points postdosing. Tumors then were processed, and tumor lysates were used to determine the inhibition of phosphorylation of AKT (pS473). Plasma was also collected, and drug concentration were analyzed. The inhibition of pAKT (left *Y*-axis) and corresponding plasma concentration of free drug (right *Y*-axis) were plotted against time points.

(25) Note: Compound **21** was not tested against human PI3Kβ. However, **21** was expected to inhibit human PI3Kβ equally potent as it inhibited other human class I PI3K isoforms.

(26) PF-04879064 was tested in a panel of 36 kinases at Invitrogen. At 1 μM, less than 25% inhibition was observed against all 36 kinases. Detailed kinome selectivity data for PF-04979064 can be found in the Supporting Information.

(27) AO clearance for the tricyclic compounds in Table 2 was also determined in the human liver cytosol assay. Human liver cytosol AO clearance data for the compounds are consistent with the clearance data from human liver S9 assay.